Available online at www.sciencedirect.com
ScienceDirect
Journal of the European Ceramic Society 32 (2012) 1301–1311
www.elsevier.com/locate/jeurceramsoc

# Atomic-level modeling and computation of intergranular glassy film in high-purity $Si_3N_4$ ceramics

Masato Yoshiya [a,b,*], Isao Tanaka [c], Hirohiko Adachi [c]

[a] Department of Adaptive Machine Systems, Osaka University, 2-1 Yamadaoka, Suita, Osaka 565-0871, Japan
[b] Nanostructure Research Laboratory, Japan Fine Ceramics Center, 2-4-1 Mutsuno, Atsuta, Nagoya 456-8587, Japan
[c] Department of Materials Science and Engineering, Kyoto University, Yoshida, Sakyo, Kyoto 606-8501, Japan

Available online 13 April 2011

**Abstract**

A model for intergranular glassy film (IGF) at grain boundaries in $Si_3N_4$ is proposed. The model agrees well with experimental information available. Although it has periodicity, atomistic simulations using the model enable to elucidate the rationale for the presence of the IGF. Amorphous models obtained by molecular dynamics based on the crystalline model enable atomistic simulations to address further issues related the IGF: it is found that the IGF plays an important role to relieve the strain due to misorientation of adjacent $Si_3N_4$ grains, that equilibrium IGF thickness is determined by the balance between the strain relief and energy penalty of silicon oxynitride constituting the IGF, and that both O and N are needed in the IGF to provide flexibility of networking structure of the IGF as well as to minimize chemical mismatch between adjacent $Si_3N_4$ grains and the IGF. Equilibrium IGF composition is successfully estimated for the first time.


*Keywords:* $Si_3N_4$; Grain boundary; Intergranular film; Simulation; Segregation

## 1. Introduction

$Si_3N_4$ based ceramic materials including their solid solutions with $Al_2O_3$, SiAlONs, are prime candidates for high-temperature structural materials due to their excellent mechanical properties at elevated temperature. $Si_3N_4$ grains are highly anisotropic, elongated ones, originated from its hexagonal crystal structure with its c/a ratio far from the value for HCP, and elongated grains are textured so that they resist crack propagation[1,2] or creep deformation.[3,4] It has been known that remarkable macroscopic properties including fracture toughness and creep resistance are often determined by characteristics of grain boundaries in spite of its negligible volume fraction. Thus, attention must be paid to optimal value of strength for bonding between grains. For example, if the bonding between grains is very strong, it improves creep resistance while it deteriorates fracture toughness since transgranular fracture takes place without any improvement by texturing of grains. On the other hand, very weak bonding between grains results in miserable creep resistance and fracture toughness since cracks propagate along grain boundaries without consuming much of the energy injected from external stress. Thus, the magnitude of bonding between grains, or grain boundaries, needs to be optimal such that the elongated grains bridge across opening gaps upon crack propagation, thereby resisting against further opening of the gap, for example. In this case friction between the elongated grains and surrounding grains governs the bridging and, in turn, fracture toughness, and the friction is determined by bonding between grains at grain boundaries. Extensive experimental studies have been conducted with success to some extent in order to improve boding between grains.[5–7] Yet further understanding of grain boundaries in $Si_3N_4$ on the atomic level is essentially needed to optimize the bonding between grains.

Transmission electron microscopy (TEM) as well as scanning TEM (STEM) has been proved to be one of powerful means to uncover grain boundaries in $Si_3N_4$. Extensive TEM observations[8–16] have revealed that an intergranular glassy film (IGF) of about 10 Å in thickness is always present at a grain boundary (two grain junctions) in sintered $Si_3N_4$, irrespective of misorientation of adjacent grains except for special boundaries.[8–11] One of the simplest explanations for its existence since early days is that the IGF is a residual matter from liquid-phase sintering. Further investigation of the IGF with

* Corresponding author at: Department of Adaptive Machine Systems, Osaka University, 2-1 Yamadaoka, Suita, Osaka 565-0871, Japan.
*E-mail address:* yoshiya@ams.eng.osaka-u.ac.jp (M. Yoshiya).

0955-2219/$ – see front matter © 2011 Elsevier Ltd. All rights reserved.
doi:10.1016/j.jeurceramsoc.2011.03.027

aids of analytical TEM demonstrated that thickness of the IGF is determined by chemistry of the IGF, instead of amount of glassy phases. High-purity $Si_3N_4$ samples, sintered by hot isostatic pressing with glass encapsulation technique, is composed of the IGFs only of 10 Å in thickness according to measurements with high statistical accuracy.[9] Oxygen atoms contained in the IGF came from oxidized surface layer of starting powder in this case. Further intentional addition of $SiO_2$ to high-purity $Si_3N_4$ does not change the IGF thickness, only results in enlargement of triple pocket (or triple grain junctions).[10] On the other hand, addition of Ca to high-purity $Si_3N_4$, for example, changes IGF thickness depending on local concentration of Ca in the IGF.[12] Other impurity elements that modify local chemistry of the IGF bring about the change in IGF thickness as well.[13,14] When grain boundaries are chemically modified, mechanical properties of a sintered body are greatly affected.[12–16] Thus, IGF thickness in Ångström order, one of the measurable properties of IGF, can be correlated with macroscopic mechanical properties. Therefore information on the atomic level about IGF is essentially needed in order to understand the characteristics of IGF, thereby controlling IGF characteristics and, in turn, macroscopic properties of $Si_3N_4$ ceramics.

Extensive chemical analyses including measurement of electronic states of the IGF by analytical TEM have provided more information on the IGF in $Si_3N_4$ than ever. Gu et al. performed detailed measurement for the IGF[17–20] by the electron energy-loss spectroscopy (EELS) which is, in part, one of elemental analysis procedures with high spatial resolution and the electron energy-loss near edge structures (ELNESs) which is an equivalent to X-ray absorption near edge structures (XANES or NEXAFS) for electron spectroscopy and can be obtained as fine structures appeared on the EELS spectrum with high energy resolution. They have revealed that the IGF is constituted by silicon oxynitride with $N/(N+O) = 0.30 \pm 0.12$,[18] instead of pure silica as believed in earlier days, and density of silicon atoms is 69.2% of that in $Si_3N_4$ grain interior.[19] In addition, they have obtained the ELNES spectrum only from the IGF which provides information on its electronic states by the spatial difference method.[20] These studies provided crucial information to model the IGF on the atomic level, which has been achieved in the first one of a series of our studies[21–26] through interpretation of the ELNES spectrum by theoretical calculations of ELNES spectrum.[21] The content of N exceeds the solubility limit of N in silica glass,[27] and thus rationale for the high nitrogen content had remained unclear until our atomistic simulation elucidated the role of N as well as O in the IGF.[26]

On the theoretical side, a pioneering work by Clarke on IGF thickness is reported.[28,29] That study tried to elucidate equilibrium thickness of the IGF in $Si_3N_4$ based on the force-balance model based on thermodynamics of diffuse interface originated from the Cahn–Hilliard theory.[30] In spite of its plausibility, the force balance model lacks atomistic description of IGF that is just as thin as a several atomic layers as pointed out by himself in the original paper.[28] Due to its strong foothold, the thermodynamic descriptions of the IGF based on the concept of diffuse interface have been flourished ever since,[28,29,31–33] though they lack atomistic description. Cannon and Esposito described IGF from viewpoint of thermodynamic adsorption of impurities on $Si_3N_4$ grains or wetting of the grains by liquid on the surface of $Si_3N_4$ grains,[34,35] which succeeded in connecting this rather special phenomenon in $Si_3N_4$ to general science and engineering of adsorption or wetting on ceramic grains surfaces based on thermodynamics. Bishop and Carter simulated the IGF at $Si_3N_4$ grain boundaries by phase-field modeling.[36]

On the atomic level, Keblinski et al. opened up a new way for atomic-level modeling of disordered grain boundary layers.[37] Although their work is confined to pure matters and thus their approach cannot be directly applied to the $Si_3N_4$ case where the IGF is constituted by silicon oxynitride, they demonstrated by molecular dynamics simulation that high-energy twist boundaries can be stabilized by disordered layers at grain boundaries. Blonski and Garofalini and Litton and Garofalini demonstrated molecular dynamics simulation on an IGF in $Al_2O_3$[38–41] which is constituted by silicate glass stable in bulk phases. However, modeling of the IGF in $Si_3N_4$ on the atomic level and atomistic simulation using the model had not been carried out until our previous studies.[22–26]

A difficulty for atomic level computations for the IGF in $Si_3N_4$ is originated from the fact that no rational model for the IGF in $Si_3N_4$ is available since (1) the IGF is constituted by silicon oxynitride that is unstable in bulk, (2) it has no periodic structure and therefore it is unable to obtain information on crystal structure from high-resolution electron microscopy (HREM) observation, and (3) the IGF is spatially confined to just about 10 Å in thickness. To overcome this difficulty, first and most importantly, the atomic-level modeling of the IGF is essentially required. Once the appropriate model is proposed, then the atomic level computation using the model can be conducted to answer following open questions about the IGF in $Si_3N_4$: (1) Why is the IGF present at grain boundaries in polycrystalline sintered $Si_3N_4$ and what role does the IGF play? (2) Why is thickness of the IGF always about 10 Å or what determines the IGF thickness? (3) Why is not the IGF pure silica or amorphous $Si_3N_4$ instead of unstable silicon oxynitride, why oxygen and nitrogen atoms coexist in the IGF, or what roles, if any, do the oxygen and nitrogen in the IGF play? To address these issues, we have carried out atomistic simulations of the IGF in $Si_3N_4$.

In this paper, we attempt to provide the broader perspective on the IGF in $Si_3N_4$ than ever, based on combination of computational techniques, especially the atomic-level picture of the IGF, rationale of its existence, and the atomic-level mechanism to accommodate $Si_3N_4$ grains with misorientation, with unpublished results of our past studies based on our challenges to reveal the nature of the IGF using atomistic simulations.[21–26] Overlapping with results in past papers is minimized as long as this paper is self-contained. Emphases are put on the modeling of the IGF itself, on answering above-mentioned open questions by atomistic simulations, and on future outlook of atomistic simulations to address further issues related to the IGF in $Si_3N_4$. Technical details of the computation in following sections are given elsewhere.[21–26]

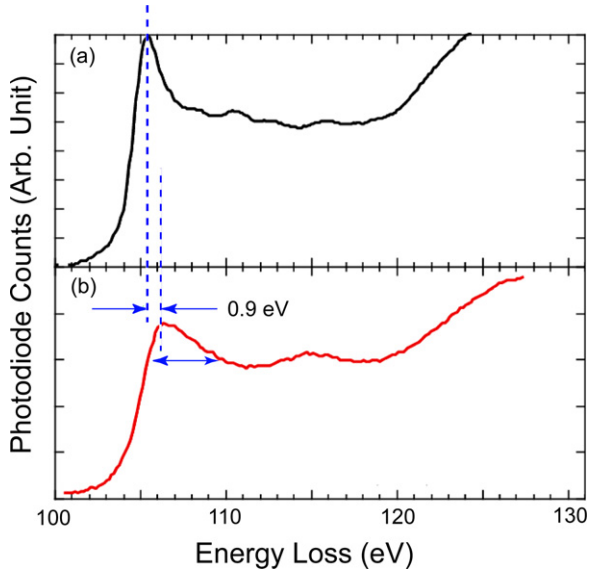


Fig. 1. Experimental ELNES spectra[20]: (a) from a $Si_3N_4$ grain and (b) from IGF obtained by the spatial difference method. Remarkable differences between two spectra are the energy shift by 0.9 eV of the first peak and broadening of the first peak in the IGF spectrum.

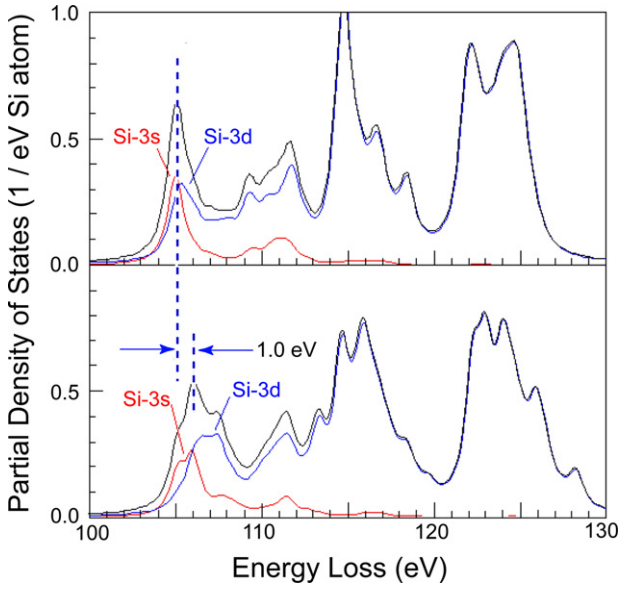


Fig. 2. Theoretical ELNES spectra obtained by ab initio DFT calculations[21]: (a) for a $Si_3N_4$ grain and (b) for the IGF. The spectra are composed of Si-3s and Si-3d partial density of states in the case of Si-$L_{2,3}$ edge. The energy shift of the first peak by 1.0 eV and the peak broadening are reproduced well.

## 2. Modeling IGF structure

According to a chemical analysis by EELS, the IGF in polycrystalline $Si_3N_4$ is composed of Si, N and O, with a N/(N + O) ratio being about 0.3–0.4, much exceeding the solubility limit of N in silica glass. Thus, it is not plausible to start modeling from the structure of silica glass. Since the IGF appears to be amorphous judging from TEM micrographs, there are many degrees of freedom in its atomic configuration with no clue about atomic coordinates. In existing crystals, $Si_3N_4$, $Si_2N_2O$, and $SiO_2$, N and O have three-fold and two-fold coordinations, respectively, while Si atoms have four-fold coordination. Assuming that coordination environment of atoms in the IGF would not be different very much from those crystals, we fixed the coordination numbers of Si, O, and N in the IGF model at 4, 2, and 3, respectively, and started modeling based on the crystal structure of β-$Si_3N_4$. Since a Si atom and a N atom are coordinated by four N atoms and three Si atoms in β-$Si_3N_4$, respectively, removing a Si from the β-$Si_3N_4$ crystal structure results in the decrease in the coordination number of the four neighboring N atoms from three to two. Then, we can substitute four O atoms for the four N atoms without introducing a dangling-bond or a broken bond since the coordination number of O is two in crystalline $SiO_2$. As a result, after one step, four tetrahedra surrounding the Si vacancy change from $SiN_4$ to $SiN_3O_1$ in β-$Si_3N_4$ structure. By repeating this step, we can increase the O content to some extent without introducing a dangling-bond until desired O content is achieved.

Comparison between experimental Si-$L_{2,3}$ edge ELNES spectra, one from $Si_3N_4$ grain and the other from the IGF, exhibited two-fold noticeable differences as shown in Fig. 1: (1) a shift of the first peak position by 0.9 eV toward higher energy side, and (2) broadening of the first peak. Although other spectral features also provide valuable information about chemical bonding between atoms in the IGF, we focused on the first peak. We started with theoretical calculations of ELNES spectra for three crystals of which structure and chemical composition are known, namely, β-$Si_3N_4$, $Si_2N_2O$ which is the only Si-based crystal where O and N coexist, and $SiO_2$ (α-quartz). All of the three crystals consist of tetrahedral units of $SiX_4$ (X = N, O), $SiN_4$ units for β-$Si_3N_4$, $SiN_3O_1$ units for $Si_2N_2O$, and $SiO_4$ units for $SiO_2$.

According to detailed analysis on the origin of the first peak based on ab initio density functional theory (DFT) calculations, it is found that the first peak corresponds to two kinds of electronic excitation, Si-2p → Si-3s and Si-2p → Si-3d, and that those two transitions are superposed in energy in β-$Si_3N_4$ and are gradually separated as O content increases.[21] The latter explains the second noticeable difference between experimental ELNES spectra: by slight separation of the two transitions, the first peak appears to be broadened. The energies of the two transition forming one or two peaks depending on O content change almost linearly with O content, and the 0.9 eV shift, the first noticeable difference between two experimental ELNES spectra, corresponds to a tetrahedral unit of $SiN_{2.1}O_{1.9}$ or N/(N + O) = 0.43. The latter agrees with the experimental chemical analysis fairly well.[18] In order to confirm that the tetrahedral unit of $SiN_{2.1}O_{1.9}$ is necessary to reproduce the ELNES spectrum from the IGF, we have carried out theoretical calculation of ELNES by ab initio DFT calculation with a model cluster of the IGF with $SiN_2O_2$ tetrahedral unit at its center. Fig. 2 compares theoretical ELNES spectra for β-$Si_3N_4$ and for the IGF. The two major differences found between experimental ELNES spectra are satisfactorily reproduced: the energy shift in theoretical ELNES spectra is 1.0 eV and the first peak is broadened.

Having confirmed that values obtained from theoretical analyses reproduce experimental results, we have substituted more O

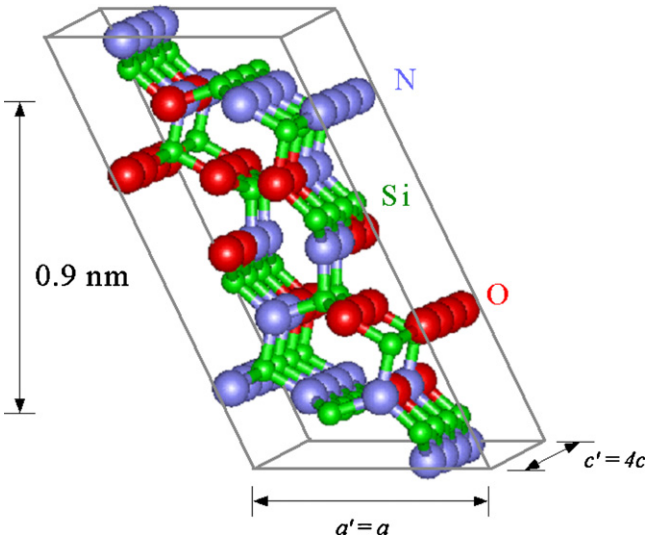


Fig. 3. The hexagonal unit cell of a model structure for the IGF which is constructed from β-$Si_3N_4$ crystal structure.[21] It is noted that no dangling-bond is contained in the model.

atoms for N atoms in the IGF model in the way mentioned above up to N/(N + O) = 0.43. These analyses through interpretation of ELNES did not have enough accuracy to determine whether N/(N + O) is close to 0.43 or 0.32. The final IGF model with N/(N + O) = 0.43 is shown in Fig. 3. Although it is hexagonal cell since the unit cell of β-$Si_3N_4$ is hexagonal, it can be easily transformed into an orthogonal cell. Length of the *c*-axis of the IGF model is four times as that in β-$Si_3N_4$ and distance between anionic layers where O and N mixture takes place is 9 Å, in good agreement with the IGF thickness measured by TEM,[8–10] although no atomic relaxation has been taken into account in this model. In addition, (1 0 $\bar{1}$ 0) prismatic plane which is typically found as edges of $Si_3N_4$ grains in TEM observation can be chosen as interfaces with $Si_3N_4$ grains by putting β-$Si_3N_4$ unit cells above and below the model. Although it is not amorphous but crystal, this model structure of the IGF enables to conduct further atomistic simulations to address issues of the IGF.

## 3. Atomistic simulations with crystalline IGF model

The first issue that has occupied minds of researchers and engineers is the question why the IGF is ubiquitous at grain boundaries of sintered high-purity $Si_3N_4$. It may be reasonable to assume it is more energetically favorable if grain boundaries are wetted with silica glass which is stable in bulk phases since its resource is abundant in sintered $Si_3N_4$: oxygen is available on surface of starting powder. One might speculate it is energetically even more favorable if grain boundaries are dry, i.e., without the IGF. These issues can be quantitatively assessed by atomistic simulations that evaluate energy of polycrystals with or without the IGF, which can be readily conducted using the model structure of the IGF proposed in the previous section. Although the IGF model structure has periodicity, not amorphous in contrast to reality, the IGF model enables to easily evaluate the atomic configuration in the IGF when it is sandwiched by two adjacent $Si_3N_4$ grains since it is based on β-$Si_3N_4$ crystal structure and thus, Si–N bonds would be similar to those in β-$Si_3N_4$ with slight modification by the presence of O, and Si–O bond length can be easily adjusted by changing Si–O–Si bond angle without introducing much strain to the crystal lattice.

To conduct atomistic simulations for the IGF, interatomic force field is needed. In this part of the study,[22] we have employed the high-accuracy potential sets for $SiO_2$ and $Si_3N_4$ reported by van Beest et al.[42] and Ching et al.[43], respectively. Both of the potential sets are obtained by ab initio calculations. Combination of these sets provides interatomic potential in the Buckingham form for Si–O, O–O, Si–N, and N–N pairs. One missing bond pair of which interatomic potential is needed for the atomistic simulation for the IGF is that between O–N, which is obtained from an extra set of ab initio DFT calculations for $Si_2N_2O$, the only one known crystal having O and N together in its structure. With fitting target of lattice constants and atomic coordinates as well as elastic constants which are obtained by giving uniaxial strain to the crystal, the interatomic potential for O–N bond is obtained in consistent with the sets for other bonds. This entire set of interatomic potentials enables to satisfactorily reproduce properties of β-$Si_3N_4$, $Si_2N_2O$, and $SiO_2$ (α-quartz), ready for the calculation of the IGF in polycrystalline $Si_3N_4$. Hereafter all the atomistic simulations in this section were carried out using GULP code.[44]

Two kinds of grain boundaries of $Si_3N_4$ were examined: one is a 0°-twist grain boundary, i.e., without misorientation between neighboring grains, and the other is a 180°-twist grain boundary. Due to high anisotropy in the crystal structure of β-$Si_3N_4$, more general misorientation could not be examined due to geometrical constraint of the model structure of the IGF. To reveal role of the IGF, two settings of the IGF for each misorientation were used: one is without the IGF or dry grain boundaries, and the other is with the IGF at the grain boundaries. Then, after sandwiching the IGF with two $Si_3N_4$ grains, structural optimizations were carried out to obtain optimized atomic coordinates and energies. One of optimized structures for the 180°-twist grain boundary with the IGF is shown in Fig. 4. Results of the excess energies calculated from energies of unstrained IGF model (only for IGF model without neighboring $Si_3N_4$ grains under three dimensional periodic boundary conditions) and $Si_3N_4$ are summarized in Fig. 5, together with schematic illustrations. Needless to say, excess energy for the dry 0°-twist grain boundary without the IGF is zero since there is actually no grain boundary. It increases to 0.40 J/$m^2$ when the IGF is inserted to the grain boundaries, and thus the IGF is energetically unfavorable when misorientation of neighboring grains is absent. In contrast, excess energy for the 180°-twist grain boundary with the IGF decreases to 0.91 J/$m^2$ from that for the dry 180°-twist grain boundary, 1.08 J/$m^2$. Thus, it is concluded that the IGF plays an important role to reduce excess energy at grain boundaries when misorientation of adjacent $Si_3N_4$ grain is present.

The origin of the reduced excess energy is evident in bond length distribution at grain boundaries: the bond lengths of Si–O and Si–N bonds have some distribution in the IGF with their respective average and their standard deviation being unchanged whether misorientation of neighboring grains is present or not, indicating that the bonds in the IGF are strained to some extent

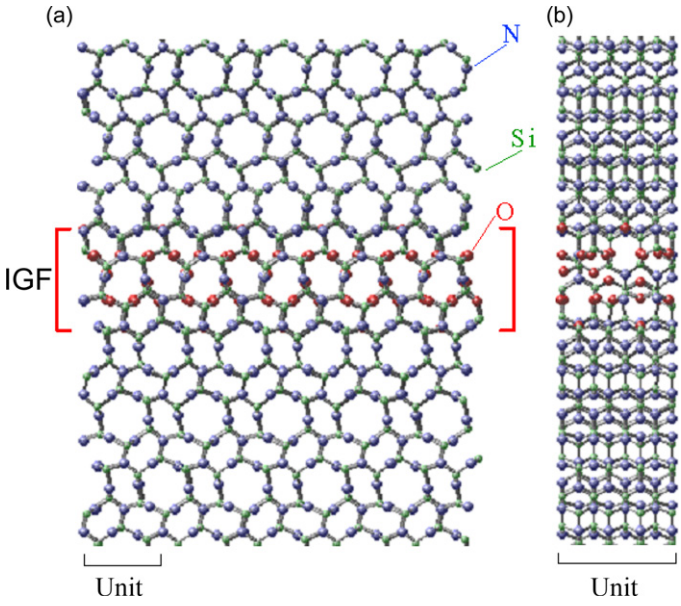


Fig. 4. One of optimized supercells projected from two directions for 180°-twist grain boundary with the crystalline IGF.[22] Five-membered ring instead of six-membered ring is formed at the center of the grain boundary in the case of 180°-twist grain boundary. It is noted that no dangling-bond is generated in the supercell upon structural optimization.

due to mixture of O and N irrespective of the misorientation. However, Si–N bond length distributions in the neighboring $Si_3N_4$ grains are significantly different from unstrained $Si_3N_4$. When the misorientation is present and the IGF is absent, Si–N bonds in the vicinity of the $Si_3N_4$/IGF interface appear to be highly strained. On the contrary, those strains of the Si–N bonds in the vicinity of the $Si_3N_4$/IGF interface are significantly relieved when the IGF is present at the grain boundary. The relief of the strain in $Si_3N_4$ grains in the vicinity of the grain boundary due to misorientation reduces excess energy at the grain boundary. In other words, the IGF plays an important role to relieve strains in neighboring $Si_3N_4$ grains imposed by misorientation of the $Si_3N_4$ grains. This justifies the presence of the IGF at grain boundaries in polycrystalline $Si_3N_4$. In spite of the simplicity of the IGF model used in this analysis, rationale for the presence of the IGF at grain boundaries in polycrystalline $Si_3N_4$ is successfully given.

## 4. Thickness of IGF determined by amorphous IGF model

In other materials, impurities are segregated not only on a grain boundary plane but also in the vicinity of a grain boundary,[45,46] although crystal lattice of matrix phases is barely changed due to segregation and thus lattice continuity breaks just on a grain boundary plane. In contrast, in the case of $Si_3N_4$, lattices of neighboring grains are separated by about 10 Å and there lies the IGF between them. Although, Clarke tried to elucidate the thickness of the IGF in the force balance model that the thickness of the IGF is determined by the balance between van der Waals attractive force between grains and steric force originating from distortion of the $SiO_4$ tetrahedra, the model did not

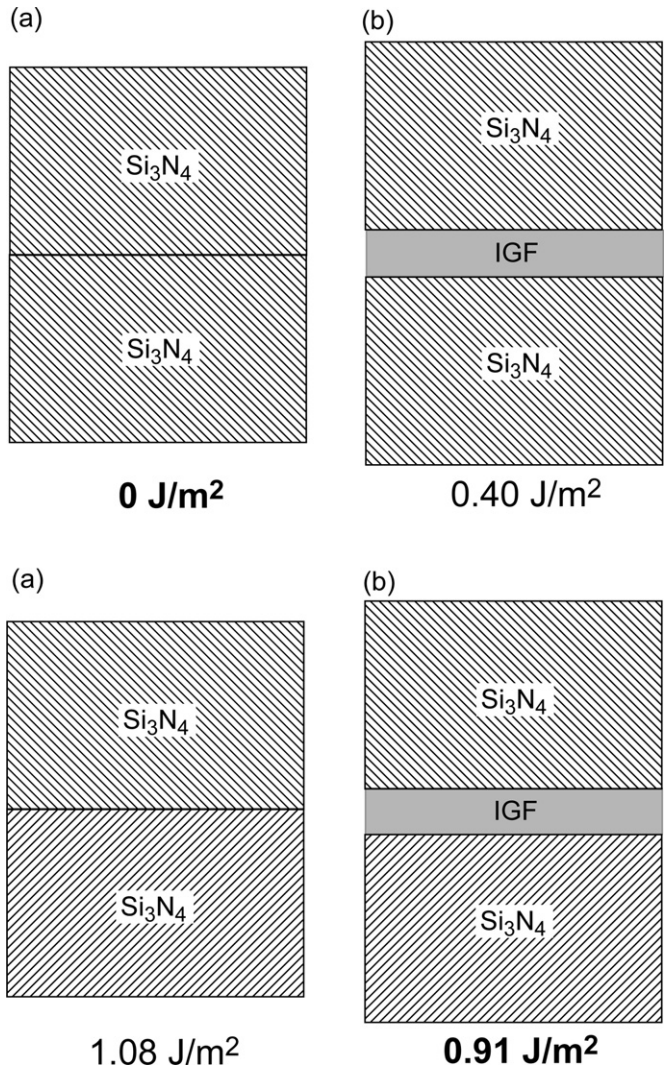


Fig. 5. Schematic drawings of dry grain boundaries and grain boundaries with the IGFs, with and without misorientation of adjacent $Si_3N_4$ grains. Although the presence of the IGF is energetically unfavorable when misorientation is absent, it is favorable when misorientation is present since the IGF relieves strain imposed on the bonding by the misorientation.

quantitatively predict the equilibrium thickness of the IGF. This issue needs to be addressed by atomistic simulations. However, the IGF model proposed in Section 2 has periodicity in its crystal structure and upper and lower ends in the model are occupied by $SiN_4$ tetrahedra instead of $SiN_xO_{4-x}$ tetrahedra, and thus it is unable to assess the IGF of which thickness is different from that determined in the model.

To overcome these difficulties, we have obtained amorphous IGF model by melting the crystalline IGF model with an aid of molecular dynamics simulations using MOLDY code.[47] This allows varying IGF thickness in the following atomistic simulations. In these simulations, more robust potential parameter set[48] is used to enable melting the silicon oxynitride at elevated temperature. The obtained structures were unchanged by further structural optimization by static energy minimization method, indicating that the obtained structures are energetically stable. It is noted that N/(N + O) ratio is fixed at 0.32 in this case. The

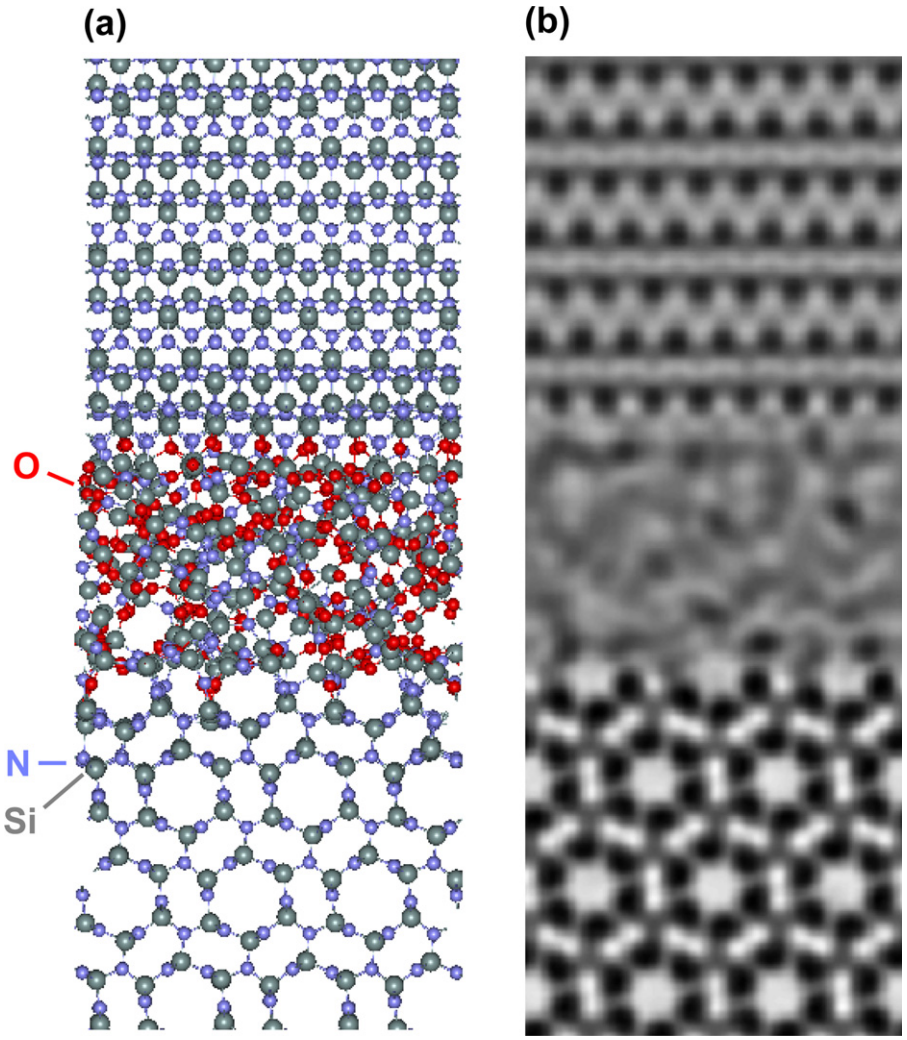


Fig. 6. (a) Ball-and-stick drawing for one of six IGF-containing 90°-twist grain boundaries of which thickness is 14.4 Å and (b) one of six simulated HREM images based on the calculated structure.[24] Due to three dimensional periodic boundary conditions, six grain boundaries are yielded by three calculations.

number of atoms contained in the supercell ranges from 4032 to 6216 depending on IGF thickness. To ensure statistical accuracy, three sets of the IGF amorphous models that differ in time length of thermalization after thermal equilibrium is achieved are used and obtained results are averaged. One of the obtained structures (the IGF thickness is 14.4 Å) is compared with simulated HREM image in Fig. 6. Although it completely looks amorphous both in the images in the figure, the detailed analysis of atomic distribution in the IGF reveals that atomic configuration is one-dimensionally ordered perpendicularly to the grain boundary.[24] It should be noted that the first layer where O and N coexists is actually ordered due to the potential field from adjacent $Si_3N_4$ grain, and thus the IGF is thicker from chemical points of view than from structural points of view, resulting in a discrepancy between HREM thickness and chemical thickness in accordance with that between experiments.[9,18]

In order to evaluate equilibrium thickness by atomistic simulations, it is necessary to consider what the IGF is in equilibrium with. In other words, it is necessary to determine reservoirs of O and N that constitute the IGF. Since the IGF is adhered to $Si_3N_4$ grains, it is no wonder that N in the IGF is in equilibrium with N in $Si_3N_4$ grains. Regarding O in the IGF, one plausible candidate is $SiO_2$ at triple pockets which terminate the IGF on both sides along a grain boundary. Taking $Si_3N_4$ and $SiO_2$ as reservoirs, or standard states, of N and O, respectively, we have evaluated grain boundary energy, $\gamma$, for various thicknesses of the IGFs. The thickness of the IGF assessed ranges from 0 (dry grain boundary) to about 40 Å, four times as experimental HREM thickness for high-purity $Si_3N_4$.

Fig. 7 shows the grain boundary energy, $\gamma$, as a function of IGF thickness, $h$, which is calculated by $h = (c - 2l)/2$ where $c$ is the length of a supercell containing two grain boundaries perpendicular to the grain boundary and $l$ is the length of unstrained β-$Si_3N_4$ slabs. Shown together in the figure by a dotted line and a broken line are components of formation energy and of strain energy, respectively. The component of formation energy, $\sigma_f$, is calculated as the formation energy per unit area of unstrained silicon oxynitride with the same composition as in the IGF based on standard states, $Si_3N_4$ and $SiO_2$. The component of strain energy, $\sigma_s$, is simply calculated by $\sigma_s = \gamma - \sigma_f$, and is equivalent to the excess energy discussed in Section 3. By definition, sum of these components is equal to grain boundary energy, $\gamma$.

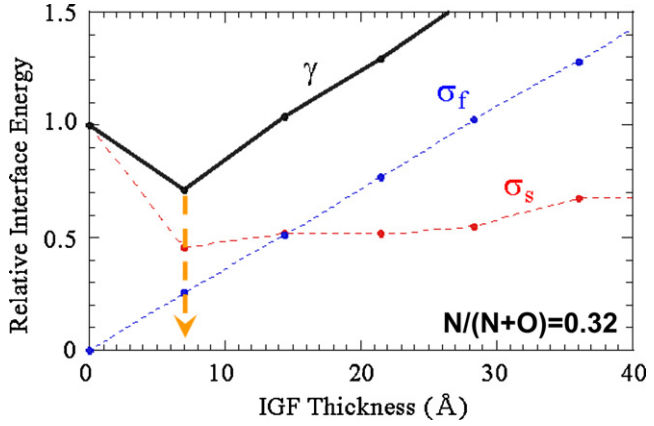


Fig. 7. Interface energy of IGF at equilibrium composition, N/(N + O) = 0.32, relative to that of dry 90°-twist grain boundary as a function of IGF thickness.[26] Components of formation energy of silicon oxynitride, $\sigma_f$, and of residual strain, $\sigma_s$, are also shown. Broken arrow indicates equilibrium IGF thickness estimated in this study.

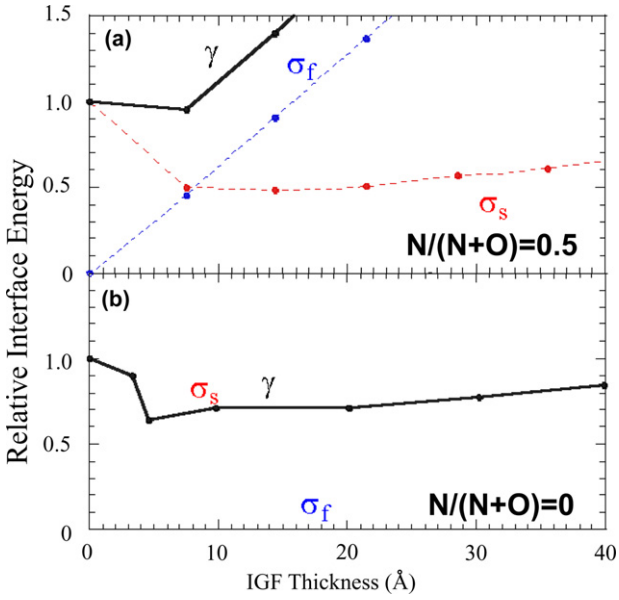


Fig. 8. Relative interface energies of IGFs with (a) excess amount of N and (b) O in the IGF as a function of IGF thickness together with components of formation energy of silicon oxynitride, $\sigma_f$, and of residual strain, $\sigma_s$.[26]

As is expected, $\sigma_f$ proportionally increases with IGF thickness, indicating that silicon oxynitride at this composition is unstable compared with macroscopic mixture of bulk $Si_3N_4$ and bulk $SiO_2$ and its energy penalty per unit area increases as its thickness, or volume, increases. This is the negative aspect of having unstable silicon oxynitride at grain boundaries. Its counterpart, $\sigma_s$, at first decreases with the increase in thickness due to relief of strain imposed by misorientation of adjacent $Si_3N_4$ grains, in accordance with the atomistic simulations using crystalline IGF model in Section 3. Then, it remains constant, or slightly increases, with further increase in thickness. This indicates that, although thin IGF is needed to relieve the strain, too thick IGF is not needed to relieve the strain. Rather thick IGF is energetically disadvantageous. Consequently, grain boundary energy, $\gamma$, which is given by sum of $\sigma_f$ and $\sigma_s$ exhibits minimum at ca. 0.7 Å in this case. This corresponds to the equilibrium thickness of the IGF and, agreement with experiments in the equilibrium thickness is satisfactory despite the fact that no experimental knowledge is used in the atomistic simulation except for empirical interatomic bonding for bulk crystals. Furthermore, these atomistic simulations provide physical insight as to what determines IGF thickness: it is determined by balance between relief of the strain due to misorientation of adjacent $Si_3N_4$ grains and energy penalty of silicon oxynitride glass. Thus, it is reasonable to expect the change in equilibrium thickness when misorientation, and in turn, the strain due to misorientation, is changed whether it is detectable in experiment or not. In fact, it is reported that equilibrium thickness at hexagonal-BN/3C-SiC exhibits remarkable dependence on grain orientation.[49]

## 5. Chemical composition of IGF

The anionic ratio in the IGF, N/(N + O), has been fixed at 0.32 in the previous atomistic simulations by which equilibrium IGF thickness is determined. The last remaining open question is the reason why both O and N are needed in the IGF in spite of the instability of silicon oxynitride or why the IGF has this anionic ratio. To answer this question, further atomistic simulations with the IGFs of different N/(N + O) ratios, namely, 0 and 0.5, in addition to 0.32, have been carried out.

Fig. 8 shows grain boundary energies for N/(N + O) = 0 and 0.5 together with the two components, $\sigma_f$ and $\sigma_s$. When N/(N + O) = 0.5, i.e., when more N is contained in the IGF, energy penalty of silicon oxynitride is higher, resulting in more steeper gradient of the slope of $\sigma_f$ than for equilibrium IGF composition, N/(N + O) = 0.32. Strain is somewhat relieved as thickness increases up to 0.8 Å, resulting in minimum of $\gamma$ at 0.8 Å. However, the strain relief is less in magnitude than that in the equilibrium IGF composition when $\sigma_s$ values at respective equilibrium thicknesses are compared. As a result, $\gamma$ is larger for N/(N + O) = 0.5 than for the equilibrium IGF composition at respective equilibrium thicknesses. This suggest that O is needed to relieve the strain due to misorientation of adjacent $Si_3N_4$ grains and the presence of O probably enables more flexible networking of Si–O–Si bonds since O has only two-fold coordination than Si–N–Si where N has three-fold coordination. On the other hand, when N/(N + O) = 0, i.e., pure silica glass, $\sigma_f$ remains at zero since it is the standard state by definition and actually it is stable. Strain is relieved as IGF thickness increases up to about 0.5 Å as indicated by $\sigma_s$ in Fig. 8(b). The magnitude of the strain relief is greater than that in equilibrium IGF composition indicated by $\sigma_s$ in Fig. 7, which is not surprising since more O atoms are contained in the IGF when N/(N + O) = 0, providing more flexibility in the networking structure. The minimal value of $\gamma$ for N/(N + O) = 0 is smaller than that of equilibrium IGF composition, N/(N + O) = 0.32. This does not explain why the IGF contains some amount of N.

To understand the details on the atomic coordination in the IGF and at the $Si_3N_4$/IGF interface, distribution of dangling bonds across the grain boundary was analyzed. Fig. 9 shows schematic illustrations of the dangling-bond distribution

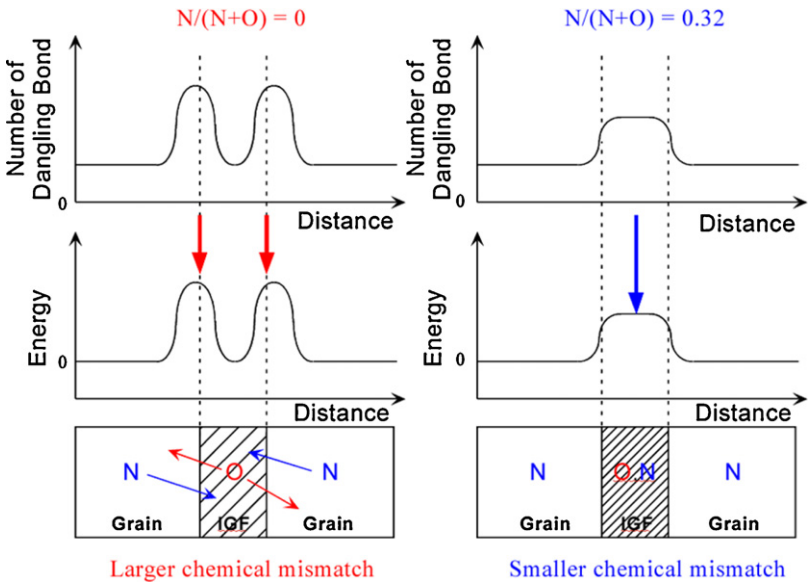


Fig. 9. Schematic drawings showing dangling-bond distribution across grain boundaries for silica IGF (left) and the IGF with equilibrium composition (right). Note that remarkable amount of dangling bonds are found at $Si_3N_4$/IGF interface when N/(N + O) = 0, drastically increasing local energy at the interfaces, while dangling-bond is almost uniformly distributed in the IGF but segregation of dangling-bonds at $Si_3N_4$/IGF is decreased when N/(N + O) = 0.32.

for N/(N + O) = 0 and 0.32. When N/(N + O) is 0.32, dangling bond is to some extent uniformly distributed in the IGF, in agreement with preceding studies for bulk matters both by computation[50] and experiments,[51,52] though close examination reveals that more dangling bonds are present at $Si_3N_4$/IGF interfaces, which predicted the crack propagation along $Si_3N_4$/IGF interface instead in the middle of the IGF.[53] On the other hand, when N/(N + O) is 0, much more number of dangling bonds are present at two $Si_3N_4$/IGF interfaces at both sides of the IGF while there is almost no dangling bond at inside of the IGF. This indicates that the presence of N in the IGF greatly reduces the dangling bond at $Si_3N_4$/IGF interface. This is probably originated from the fact that the number density of interatomic bonds in $Si_3N_4$ is much greater than in $SiO_2$. Thus, N is necessary to reduce chemical mismatch between $Si_3N_4$ and the IGF. To reduce the local energy penalty at $Si_3N_4$/IGF interface, N would go into the IGF and O would go into $Si_3N_4$ grains, resulting in the increase in IGF thickness and N/(N + O) ratio of the IGF.

The failure of predicting equilibrium IGF composition based on $\gamma$ values in spite of the local dangling-bond analysis that suggest mixing of O and N in the IGF can be attributed in part to the fact that respective equilibrium IGF thicknesses are different and thus the numbers of atoms in respective IGFs are different. Another possibility is that energy penalty of silicon oxynitride might be overestimated and/or entropy term contribution is neglected in this study: the interatomic potential set used in these atomistic simulation is not designed for silicon oxynitride glass with high N/(N + O) ratio and the equilibrium IGF thickness evaluated in the previous section is smaller than experimental value. If the energy penalty of silicon oxynitride is halved, for example, the equilibrium IGF thickness would be estimated at 10 Å, in perfect agreement with experiment. In that case, $\gamma$ for N/(N + O) = 0 becomes greater than that for N/(N + O) = 0.32, equilibrium IGF composition. However, we cannot neglect the fact that equilibrium IGF thickness is dependent on the IGF composition and thus the numbers of atoms representing the excess energy at grain boundaries are different.

To quantitatively compare excess energies at grain boundaries as a function of the IGF composition, atomic excess energy, $\varepsilon$, is calculated as

$$\varepsilon = \frac{\gamma A}{N}$$

where $A$ is area of grain boundary plane and $N$ is the number of atoms in the IGF. The atomic excess energy is plotted as a function of anionic ratio of the IGF in Fig. 10. The atomic excess energy roughly corresponds to chemical potential of atoms in the IGF and it is minimal when the IGF is at equilibrium chemical composition, suggesting that equilibrium IGF composition is the one where N/(N + O) = 0.32. This does not change the rationale for the existence of O and N in the IGF: O is necessary in

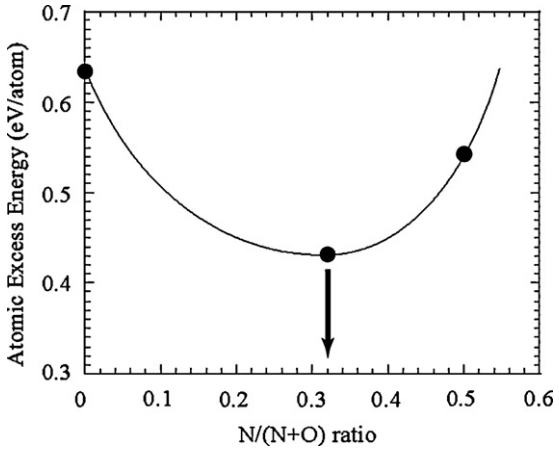


Fig. 10. Atomic excess energy as a function of anionic ratio of the IGF, N/(N + O). The arrow indicates equilibrium IGF thickness in perfect agreement with experiment.[18]

the IGF to provide more flexibility in its network structure and N is necessary in the IGF to minimize the chemical mismatch with $Si_3N_4$ grains, and that the equilibrium IGF composition is determined by the balance between these roles of O and N.

It is still an open question as to which of $\gamma$ or $\varepsilon$ determines the equilibrium IGF composition. It is related to the question as to how locally energy and state of a matter can be determined. To authors' best knowledge, non-equilibrium thermodynamics that assumes local equilibrium does not state about the actual size of the local region and thus do not answer this question. If the local region is composed only of an atom and atom moves to neighboring region or from/to reservoir based on the local energy as in grand canonical ensemble simulations, which it seems likely to the authors, the equilibrium IGF composition is determined of $\varepsilon$ instead of $\gamma$. Consequently, the IGF having N more than solubility limit is more energetically favorable than the IGF composed of pure silica.

## 6. Summary and outlook

Modeling of the IGF on the atomic level was demonstrated and atomistic simulations using the crystalline and amorphous IGF models were carried out. It is found that the IGFs are needed at grain boundaries to relieve the strain imposed by misorientation of adjacent $Si_3N_4$ grains, that the equilibrium thickness of the IGF is determined by the balance between the strain relief and energy penalty of silicon oxynitride, that O is necessary in the IGF to provide more flexibility in its networking structure and in turn more ability to relieve the strain and N is necessary in the IGF to minimize chemical mismatch with neighboring $Si_3N_4$ grains.

The next issue that should be addressed is the influence of impurity element in the IGF on bonding of $Si_3N_4$ grains via IGF and atomic arrangement in the IGF and at IGF/$Si_3N_4$ interface. Recent progress in spatial resolution of TEM or STEM enables to analyze the IGF in atomic resolution and to detect impurity elements at $Si_3N_4$/IGF interface.[54–58] However, from practical points of view, it requires the impurities to be ordered to be detected by Z-contrast imaging and difference in atomic number needs to be large. Even now, it is still challenging to analyze impurities that are distributed in the silicon oxynitride IGF, which modifies the networking structure, thereby changing the properties of the IGF. Therefore, there is still plenty rooms for atomistic simulation, whether classical or quantum, to play roles to unveil the nature of the IGF.

Following our studies, atomistic simulations for impurity-containing IGF in $Si_3N_4$[59–61] as well as grand canonical Monte Carlo simulations[62] using empirical interatomic potential sets have been demonstrated. Besides, ab initio calculations have been demonstrated to examine very local atomic configuration as well as chemical bonding between atoms modified by the impurities.[63–67] Both categories of computations succeeded to some extent, well enough to extend our knowledge on the IGF. However, for more quantitative understanding of the IGF modified by impurities, we must keep in mind that chemical bonding between atoms would be modified by impurities and thus empirical interatomic potential parameter sets might be unable to predict unknown states of the IGF with impurities, requiring more chemically flexible potential sets, and that attention mush be paid to geometrical constraints by neighboring $Si_3N_4$ grains upon predicting realistic states of the IGF with impurities by ab initio calculation, requiring far larger supercell containing much more number of atoms than those used today. Although these requirements are hard to be satisfied today, further development of computational resources would enable them in a straightforward manner. Finally, it is not sufficient to reveal the states of the IGF with impurities but it is essentially needed to reveal underlying physics that determine the states of the IGF with impurities as attempted in this series of our studies. When the underlying physics is clarified and a clue to control it is obtained, it enables not only to optimize boding between grains thereby tailoring this series of materials through improving creep resistance and fracture toughness, but also to improve other properties such as optical properties, thermal properties, and so on.

## Acknowledgment

This study is in part supported by Grant-in-Aid for Scientific Research on Priority Areas "Atomic Scale Modification" (No. 474) from the Ministry of Education, Culture, Sports, Science and Technology, Japan.

## References

1. Becher PF, Hwang SL, Lin HT, Tiegs TN. Microstructural contribution to the fracture resistance of silicon nitride ceramics. In: Hoffmann MJ, Petzow G, editors. *Tailoring of mechanical properties of $Si_3N_4$ ceramic*. Dordrecht, The Netherlands: Kluwer Academic Publishers; 1994. p. 87–100.
2. Šajgalik P, Dusza J, Hoffmann M. Relationship between microstructure toughening mechanisms, and fracture toughness of reinforced silicon nitride ceramics. *J Am Ceram Soc* 1995;**78**:2619–24.
3. Wilkinson DS. Creep mechanism on silicon nitride ceramics. In: Hoffmann MJ, Petzow G, editors. *Tailoring of mechanical properties of $Si_3N_4$ ceramic*. Dordrecht, The Netherlands: Kluwer Academic Publishers; 1994. p. 327–38.
4. Jing Q, Wilkinson DS, Weatherly GC. High-resolution electron microscopy investigation of viscous flow creep in a high purity silicon nitride. *J Am Ceram Soc* 1999;**82**:1492–6.
5. Becher PF, Sun EY, Plucknett KP, Alexander KB, Hsueh CH, Lin HT, et al. Microstructural design of silicon nitride with improved fracture toughness: I. Effect of grain shape and size. *J Am Ceram Soc* 1998;**81**:2821–30.
6. Sun EY, Becher PF, Plucknett KP, Hsueh CH, Alexander KB, Waters SB. Microstructural design of silicon nitride with improved fracture toughness: II. Effects of yttria and alumina additives. *J Am Ceram Soc* 1998;**81**:2831–40.
7. Becher PF, Painter GS, Sun EY, Hsueh CH, Lance MJ. The importance of amorphous intergranular films in self-reinforced $Si_3N_4$ ceramics. *Acta Mater* 2000;**48**:4493–9.
8. Kleebe HJ, Hoffmann MJ, Rühle M. Influence of secondary phase chemistry of grain-boundary film thickness in silicon-nitride. *Z Metallkd* 1992;**83**:610–7.
9. Kleebe HJ, Cinibulk MK, Cannon RM, Rühle M. Statistical-analysis of the intergranular film thickness in silicon-nitride ceramics. *J Am Ceram Soc* 1993;**76**:1969–77.
10. Kleebe HJ, Cinibulk MK, Tanaka I, Bruley J, Vetrano JS, Rühle M. High resolution electron microscopy studies on silicon nitride ceramics. In: Hoffmann MJ, Petzow G, editors. *Tailoring of mechanical properties of $Si_3N_4$ ceramic*. Dordrecht, The Netherlands: Kluwer Academic Publishers; 1994. p. 259–74.

11. Knowles KM, Turan S. Atomic structure of a Σ9 <0 1 1> $Si_3N_4$ tilt grain boundary. *Mater Sci Forum* 1996;**207–209**:353–6.
12. Tanaka I, Kleebe HJ, Cinibulk MK, Bruley J, Clarke DR, Rühle M. Calcium concentration dependence of the intergranular film thickness in silicon nitride. *J Am Ceram Soc* 1994;**77**:911–4.
13. Pezzotti G, Ota K, Kleebe HJ. Viscous slip along grain boundaries in chlorine-doped silicon nitride. *J Am Ceram Soc* 1997;**80**:2341–8.
14. Wang CM, Pan X, Hoffmann MJ, Cannon RM, Rühle M. Grain boundary films in rare-earth-glass-based silicon nitride. *J Am Ceram Soc* 1996;**79**:788–92.
15. Hoffmann MJ, Gu H, Cannon RM. Influence of the interfacial properties on the microstructural development and properties of silicon nitride ceramics. *Mater Res Soc Symp Proc* 2000;**586**:65–74.
16. Tanaka I, Igashira K, Kleebe HJ, Rühle M. High-temperature strength of fluorine-doped silicon nitride. *J Am Ceram Soc* 1994;**77**:275–7.
17. Gu H. Chemistry and bonding of grain boundary and interface in silicon nitride based ceramic materials. In: *Interface science and materials interconnection.* Sendai, Japan: The Japan Institute of Metals; 1996. p. 217–20.
18. Gu H, Cannon RM, Rühle M. Composition and chemical width of ultrathin amorphous films at grain boundaries in silicon nitride. *J Mater Res* 1998;**13**:376–87.
19. Gu H. Quantitative interfacial chemistry and bonding in ceramic materials. *Mater Res Soc Symp Proc* 1997;**453**:703.
20. Gu H, Čeh M, Stemmer S, Müllejans H, Rühle M. A quantitative approach for spatially-resolved electron energy-loss spectroscopy of grain boundaries and planer defects on a subnanometer scale. *Ultramicroscopy* 1995;**59**:215–27.
21. Yoshiya M, Adachi H, Tanaka I. Interpretation of Si-$L_{2,3}$ edge electron energy loss near edge structures (ELNES) from intergranular glassy film of $Si_3N_4$ ceramics. *J Am Ceram Soc* 1999;**82**:3231–6.
22. Yoshiya M, Tanaka I, Adachi H. Energetical role of modeled intergranular glassy film in $Si_3N_4$–$SiO_2$ ceramics. *Acta Mater* 2000;**48**:4741–5.
23. Tanaka I, Yoshiya M, Nishitani SR, Adachi H. Intergranular glassy films in $Si_3N_4$–$SiO_2$ ceramics: morphology, chemistry atomic structure, and energetics. *Ceram Trans* 2000;**118**:445–52.
24. Yoshiya M, Tanaka I, Adachi H, Cannon RM. Theoretical study on the structure and energetics of intergranular glassy film in $Si_3N_4$–$SiO_2$ ceramics. *Int J Mater Res* 2010;**101**:57–65.
25. Yoshiya M, Tatsumi K, Tanaka I, Adachi H. Molecular dynamics study of intergranular glassy film in high-purity $Si_3N_4$–$SiO_2$ ceramics. *Ceram Trans* 2000;**118**:453–70.
26. Yoshiya M, Tatsumi K, Tanaka I, Adachi H. Theoretical study on the chemistry of intergranular glassy film in $Si_3N_4$–$SiO_2$ ceramics. *J Am Ceram Soc* 2002;**85**:109–12.
27. Gu H, Cannon RM, Seifert HJ, Hoffmann MJ, Tanaka I. Solubility of $Si_3N_4$ in liquid $SiO_2$. *J Am Ceram Soc* 2002;**85**:25–32.
28. Clarke DR. On the equilibrium thickness of intergranular glass phases in ceramic materials. *J Am Ceram Soc* 1987;**70**:15–22.
29. Clarke DR, Shaw TM, Philipse AP, Horn RG. Possible electrical double-layer contribution to the equilibrium thickness of intergranular glass-film in polycrystalline ceramics. *J Am Ceram Soc* 1993;**76**:1201–4.
30. Cahn JW, Hilliard JE. Free energy of a nonuniform system. I. Interfacial free energy. *J Chem Phys* 1958;**28**:258–67.
31. Clarke DR. The intergranular film in silicon nitride ceramics – a diffuse interface approach. In: Hoffmann MJ, Petzow G, editors. *Tailoring of mechanical properties of $Si_3N_4$ ceramic*. Dordrecht, The Netherlands: Kluwer Academic Publishers; 1994. p. 291–301.
32. Bishop CM, Cannon RM, Carter WC. A diffuse interface model of interfaces: grain boundaries in silicon nitride. *Acta Mater* 2005;**53**:4755–64.
33. Bobeth M, Clarke DR, Pompe W. A diffuse interface description of intergranular films in polycrystalline ceramics. *J Am Ceram Soc* 1999;**82**:1537–47.
34. Cannon RM, Esposito L. High temperature colloidal behavior: particles in liquid silicates. *Z Metallkd* 1999;**90**:1002–15.
35. Cannon RM, Rühle M, Hoffmann MJ, French RH, Gu H, Tomsia AP, et al. Adsorption and wetting mechanisms at ceramic grain boundaries. *Ceram Trans* 2000;**118**:427–44.
36. Bishop CM, Carter WC. Relating atomistic grain boundary simulation results to the phase-field model. *Comput Mater Sci* 2002;**25**:378–86.
37. Keblinski P, Phillpot SR, Wolf D, Gleiter H. Thermodynamic criterion for the stability of amorphous intergranular films in covalent materials. *Phys Rev Lett* 1996;**77**:2965–8.
38. Blonski S, Garofalini SH. Molecular dynamics study of silica–alumina interfaces. *J Phys Chem* 1996;**100**:2201–5.
39. Blonski S, Garofalini SH. Atomistic structure of calcium silicate intergranular films in alumina studied by molecular dynamics simulations. *J Am Ceram Soc* 1997;**80**:1997–2004.
40. Litton DA, Garofalini SH. Atomistic structure of sodium and calcium silicate intergranular films in alumina. *J Mater Res* 1999;**14**:1418–29.
41. Litton DA, Garofalini SH. Molecular dynamics simulations of calcium aluminosilicate intergranular films on (0 0 0 1) $Al_2O_3$ facets. *J Am Ceram Soc* 2000;**83**:2273–81.
42. van Beest BWH, Kramer GJ, van Santen RA. Force fields for silicas and aluminophosphates based on ab-initio calculations. *Phys Rev Lett* 1990;**64**:1955–8.
43. Ching WY, Xu YN, Gale JD, Rühle M. Ab-initio total energy calculation of alpha- and beta-silicon nitride and the derivation of effective pair potentials with application to lattice dynamics. *J Am Ceram Soc* 1998;**81**:3189–96.
44. Gale JDGULP. A computer program for the symmetry-adapted simulation of solids. *J Chem Soc Faraday Trans* 1997;**93**:629–37.
45. Oyama T, Yoshiya M, Matsubara H, Katsuyuki M. Numerical analysis of solute segregation at Σ5 (3 1 0)/[0 0 1] symmetric tilt grain boundaries in $Y_2O_3$-doped $ZrO_2$. *Phys Rev B* 2005;**71**:224105.
46. Yoshiya M, Oyama T. Impurity and vacancy segregation at symmetric tilt grain boundaries in $Y_2O_3$-doped $ZrO_2$. *J Mater Sci* 2011;**46**:4176–90.
47. Refson K. Molecular-dynamics simulation of solid N-butane. *Physica B* 1985;**131**:256–66.
48. Unuma H, Kawamura K, Sawaguchi N, Maekawa H, Yokokawa T. Molecular-dynamics study of Na–Si–O–N oxynitride glasses. *J Am Ceram Soc* 1993;**76**:1308–12.
49. Knowles KM, Turan S. The dependence of equilibrium film thickness on grain orientation at interphase boundaries in ceramic–ceramic composites. *Ultramicroscopy* 2000;**83**:245–59.
50. Umesaki N, Hirosaki N, Hirao K. Structural characterization of amorphous silicon nitride by molecular dynamics simulation. *J Non-Cryst Solids* 1992;**150**:120–5.
51. Behrens KM, Klinkenberg ED, Finster J, Meiwes-Broer KH. Geometric structure of thin $SiO_xN_y$ films on Si(1 0 0). *Surf Sci* 1998;**402–404**:729–33.
52. He LN, Inokuma T, Hasegawa S. Properties of 'stoichiometric' silicon oxynitride films. *Jpn J Appl Phys* 1996;**35**:1503–8.
53. Ii S, Iwamoto C, Matsunaga K, Yamamoto T, Yoshiya M, Ikuhara Y. Direct observation of intergranular cracks in sintered silicon nitride. *Philos Mag* 2004;**84**:2767–75.
54. Ziegler A, Kisielowski C, Hoffmann MJ, Ritchie RO. Atomic resolution transmission electron microscopy of the intergranular structure of a $Y_2O_3$-containing silicon nitride ceramic. *J Am Ceram Soc* 2003;**86**:1777–85.
55. Ziegler A, Idrobo JC, Cinibulk MK, Kisielowski C, Browning ND, Ritchie RO. Interface structure and atomic bonding characteristics in silicon nitride ceramics. *Science* 2004;**306**:1768–70.
56. Shibata N, Pennycook SJ, Cosnell TR, Painter GS, Shelton WA, Becher PF. Observation of rare-earth segregation in silicon nitride ceramics at subnanometre dimensions. *Nature* 2004;**428**:730–3.
57. Winkelman GB, Dwyer C, Hudson TS, Nguyen-Manh D, Döblinger M, Satet RL, et al. Three-dimensional organization of rare-earth atoms at grain boundaries in silicon nitride. *Appl Phys Lett* 2005;**87**:061911.
58. Shibata N, Painter GS, Becher PF, Pennycook SJ. Atomic ordering at an amorphous/crystal interface. *Appl Phys Lett* 2006;**89**:051908.
59. Garofalini SH, Luo WJ. Molecular dynamics simulations of calcium silicate intergranular films between silicon nitride crystals. *J Am Ceram Soc* 2003;**86**:1741–52.
60. Su X, Garofalini SH. Role of nitrogen on the atomistic structure of the intergranular film in silicon nitride: a molecular dynamics study. *J Mater Res* 2004;**19**:3679–87.

61. Su X, Garofalini SH. Effect of interphase mixing on the structure of calcium silicate intergranular film/silicon nitride crystal interfaces. *J Appl Phys* 2005;**97**:113526.
62. Hudson TS, Nguyen-Manh D, van Duin ACT, Sutton AP. Grand canonical Monte Carlo simulations of intergranular glassy films in beta silicon nitride. *Mater Sci Eng A* 2006;**422**:123–35.
63. Chen J, Rulis P, Ouyang L, Misra A, Ching WY. Complex nonlinear deformation of nanometer intergranular glassy films in β-$Si_3N_4$. *Phys Rev Lett* 2005;**95**:256103.
64. Rulis P, Chen J, Ouyang L, Ching WY, Su X, Garofalini SH. Electronic structure and bonding of intergranular glassy films in polycrystalline $Si_3N_4$: ab initio studies and classical molecular dynamics simulations. *Phys Rev B* 2005;**71**:235317.
65. Painter GS, Becher PF, Kleebe HJ, Pezzotti G. First-principles study of the effects of halogen dopants on the properties of intergranular films in silicon nitride ceramics. *Phys Rev B* 2002;**65**:064113.
66. Painter GS, Becher PF, Chelton WA, Satet RL, Hoffmann MJ. First-principles study of rare-earth effects on grain growth and microstructure in β-$Si_3N_4$ ceramics. *Phys Rev B* 2004;**70**:144108.
67. Painter GS, Averill FW, Becher PF, Shibata N, van Benthem K, Pennycook SJ. First-principles study of rare earth adsorption at β-$Si_3N_4$ interfaces. *Phys Rev B* 2008;**78**:214206.